Cyclically-Induced Pore Pressure at High Confining Stress

by

Michael K. Sharp[1] and R. Scott Steedman[2]

ABSTRACT

Experiments were conducted by the ERDC Centrifuge Research Team to investigate effective confining stress effects on liquefaction potential of fine, clean, Nevada sand, under the boundary and loading conditions of a centrifuge model. For this test series, twenty-six level ground models with either a dense layer over a loose layer or homogeneous profile were tested in an equivalent-shear-beam box. Some models were subjected to sequential earthquakes, and some models were overconsolidated, to observe stress-history effects on pore pressure development. The purpose of this paper is to make the initial liquefaction and confining stress studies, centrifuge test procedures, results, and validation efforts conducted to date known to the professional community.

KEYWORDS: Centrifuge; confining stress; dams; earthquakes; liquefaction; pore-pressure

1.0 INTRODUCTION

The concern over earthquake resistance of older embankment dams drives the need for remedial construction costing hundreds of millions of dollars of public funds annually. This concern is not generated by actual experience from failures of well-designed dams but from predictions based on scientifically sound principles of soil mechanics. Yet the mechanical response of an embankment dam depends on so many factors that interact non-linearly that implementation of these principles in a predictive tool is still as much an art as it is a science. Thus the decision-maker is faced with the dilemma of making large investments in the absence of experience versus protecting the public from the catastrophic consequences that loss of a major dam would entail.

Liquefaction is the most critical factor to the earthquake resistance of embankment dams. Foundation materials that are structurally ideal under static loading can be severely weakened by pore pressures induced from earthquake motions. Many dams built before awareness of liquefaction must now be reexamined in light of potential damage from this threat. An open question in these reexaminations is the effect of depth on liquefaction potential. Historically, there have been no observations of liquefaction at depths greater than about 30 m or 100 ft (as summarized in Youd and Idriss, 1997), suggesting that the high confining stress beneath most embankment dams wound not be conducive to significant pore pressure response. If so, remedial construction could be avoided or simplified in many dams now under investigation. Studies to investigate these and other liquefaction questions relevant to earth dams are in progress at the U.S. Army Corps of Engineers, Engineering Research and Development Center (ERDC), Vicksburg, MS. Recent findings, focused on level ground stress conditions, are reported in this paper.

2.0 ERDC CENTRIFUGE TESTS

This section describes the test plan, description of the soils tests, equipment used to conduct the tests, as well as model construction, quality control and instrumentation. The results and an interpretation of results conclude the section.

[1] Centrifuge Research Center, Engineer Research and Development Center, Vicksburg MS (USA)
[2] Whitby Byrd and Associates, London England (UK)

2.1 Test Plan

The centrifuge experiments, summarized in Table 1, were designed to investigate liquefaction potential of a loose, saturated sand layer with initial vertical effective confining stresses ranging from 1 to 10 atm. Level ground stress conditions were used in all tests. As shown in Table 1, the models are grouped in series that correspond to different target ranges of vertical effective overburden stress near the bottom of the deposit. All models were shaken initially at a 50g spin rate with subsequent shakings at either 50g, 80g, 100g, or 125g. The results reported in this paper concentrate on the first shakings at 50g, unless specifically stated otherwise. Some models were overconsolidated by a factor of 2.5 prior to shaking (achieved by running the centrifuge up to 125g, then back down to 50g for the shaking event).

Table 2 provides further details on each experiment, including the densities achieved in the specimen, the number of earthquake events and the initial vertical effective stress near the bottom of the deposit. For the two-layer models, the target relative density for the upper medium dense layer was 75 percent while the target relative density for the lower layer was 50 percent. For the uniform deposits, the target relative density was 50 percent.

The cross-sections for the different series of experiment are shown in Figure 1. A variety of techniques were used to achieve higher confining stresses while maintaining the same g level. In some specimens, the water table or phreatic surface was lowered; in others a surcharge (lead weights) was added on the surface.

The thickness of the loose sand layer, for the two-layer case, was constant in all the experiments (160mm or 8m equivalent field thickness when tested at 50g). The thickness of the overlying deposits, and selection of water table or surcharge were adjusted to achieve the target effective vertical stress at its mid-depth. The overall depth of sand within each specimen was either 300mm or 525mm (15m or 26.25m respectively, when tested at 50g).

2.2 Soils Used in Centrifuge Models

The Nevada sand used in the models was characterized by standard laboratory tests to determine parameters such as dry density and gradation. The constitutive behavior for Nevada sand based on laboratory triaxial and simple tests is given by (Arulmoli et al., 1992). These tests show the typical reduction with K_σ at elevated confining pressure. As a reference, the K_σ relationship for this sand is shown in Figure 2, which clearly displays the effect of confining pressure. A linear extrapolation of cyclic strength from low confining pressures would result in over estimates of the available strength at high confining stresses.

2.3 Pore Fluid

All models were saturated with a glycerin-water solution which comprised an 80 percent by weight mixture of glycerin and water, determined after study of the sensitivity of the viscosity to changes in temperature and the mix proportions, Steedman (1999). The viscosity of the fluid at 1g was selected to maintain proper scaling of the permeability at 50g. Tables 3 and 4 present key material parameters for Nevada sand, and the glycerin-water solution respectively.

The density of the glycerine-water mix was calculated from as follows.

$$\rho_m = \rho_g(m_g + m_w)/(m_g + \rho_g m_w)$$

In this equation ρ_m is the density of the mix, ρ_g is the density of glycerine, m_g is the mass of glycerine, and m_w is the mass of water.

2.4 Earthquake Simulation

The earthquake actuator used in the ERDC experiments is a mechanical shaker designed to provide a single frequency input motion of variable duration to the base of the specimen container. The displacement of the platform is

constant at +/- 1mm; the frequency and hence amplitude is readily changed by varying the speed of the shaft. The use of a single frequency of input motion facilitates comparisons with laboratory tests and practical liquefaction analysis procedures based on equivalent, uniform cycles. Table 5 gives the pertinent characteristics of the input motion for each model reported in this paper.

2.5 Equivalent Shear Beam Model Container (ESB)

The soil specimen is built within a hollow rectangular model container (termed an equivalent shear beam, or ESB container) comprised of a series of aluminum alloy rings stacked one above the other, and separated by an elastic medium. Several of these chambers have been constructed, and extensive dynamic analysis and testing have been carried out to determine their dynamic response characteristics (Butler 1999).

The ESB concept is to create an equivalent shear beam with an average stiffness comparable to the stiffness of the soil specimen during the initial stages of the shaking, so that the dynamic response of the box does not significantly influence the behavior of the soil specimen inside. A chamber with no stiffness simply adds mass to the soil specimen, again changing its dynamic response. In experiments involving liquefaction of large volumes of soil inside the container, the stiffness (and hence dynamic response) of the soil changes throughout the base shaking.

The ERDC ESB model container has internal dimensions of 627mm deep by 315mm wide by 796mm long. Each of the 11 aluminum alloy rings was 50 mm high and had a plan area of 0.0675 m^2. The rings are not stiff enough along their long dimension to support the outward pressure from the soil inside under high g, therefore the container relies on vertical reaction walls, independent of the shaker unit itself, for lateral support. A rubber sheet separates the rings from the steel walls on either side, and is designed to be incompressible but very flexible in shear. This system has undergone extensive study to verify that the ESB box is not being impeded from moving with the shaker platform even though the container expands during spin up to 50 g and sits snugly against the reaction walls.

The end walls of the ESB have thin metal sheets, termed shear sheets, fixed securely to the base of the chamber, Steedman et al. (2000). The shear sheets transmit the complementary shear force generated by the horizontal shaking on vertical planes within the specimen to the base of the container. This improves the uniformity of the stress field at each elevation along the model, reducing the tendency for the chamber to rock thus better representing the stress state boundary condition that exists in the field.

Butler (1999) conducted a thorough theoretical and experimental analysis of the dynamic response of the coupled soil-container system. At high g the soil and container act as a coupled system, where the lower stiffness of the container reduces the natural frequency (slightly) of the combined system compared to the soil column alone. However, provided the driving frequency is low relative to the natural frequency of the coupled system, Butler (1999) demonstrated that the displacement response of the system is unaffected compared to the soil acting independently.

2.6 Model Construction

The specimens were all 300mm wide and 781mm long, between the vertical sidewalls of the ESB. The specimen was constructed within the ESB container by pluviating dry Nevada sand, forming a level sand bed. Instruments were placed at different depths, during the pluviation process, to measure pore pressures and accelerations. The volume and density of sand poured for each layer was checked to verify the target relative density. Once complete, the specimen was fully submerged by introducing the viscous fluid into the model from the bottom by gravity over a period of several days.

As the equivalent field depth was increased in successive experiments, the options were to shake the models at a higher g level (spin rate),

to depress the water table or phreatic surface, or to use surcharging to achieve the target overburden. It was determined that the models should all be shaken at 50g, and that surcharging would be adopted to reach the required stress levels. In the Model 4 series, two models used a depressed phreatic surface and two used surcharging. In the Model 5 series, the equivalent field depth was too great to be achieved without surcharging. The surcharge comprised lead strips laid lengthwise along the surface of the specimen, with additional lead plate on top where necessary. The phreatic surface was then maintained at the surface of the sand bed.

The centrifuge was operated at 50g (for the majority of tests reported in this paper unless otherwise specified), creating a field-equivalent of a site approximately 40 m long by 15 m wide by over 26 m deep (for the deepest specimens). Surcharges, variations in the depth of the phreatic surface, and increased g level were used to achieve higher effective overburden stresses, up to 10 atm, as described earlier.

3.0 EXPERIMENTAL RESULTS

In the initial experiment series, Table 2 (model code 2a – 2f), the behavior of a soil column 15m deep, with about 1 atm vertical effective stress in the lower layer was studied. The soil deposit had a 7m thick upper layer of denser Nevada sand (relative density of 73 to 83 percent), and a lower layer of looser sand (relative density of 43 to50 percent). The entire model was fully submerged. Example results for this model series are shown in Figure 3, for model 2f. This model has an overconsolidation ratio of 2.5. The effect of overconsolidation for this series was to slow the rate of pore pressure increase throughout the column. Accelerometer records are shown for depths of 1.5, 3.8, 6.5, 11.3, 14.5, and 15m. Pore pressure transducer records are shown for depths of 3.5, 6.9, 11, and 14.8m. The input motions are applied at 0.54 Hz, and the fundamental period of the soil column is estimated to be 4x15m/300mps = 0.2 seconds.

Pore pressures begin to rise simultaneously at all 4 transducer depths at 1.5 cycles or 3 seconds of shaking. During this time, the accelerations are ramping up to 0.10g uniformly in the 4 upper accelerometers, and to 0.12g in the input motion at 15m and the deepest accelerometer at 14.5m. At 7.8 seconds, acceleration peaks at 0.18g for 1.5m, and at 0.15g for 3.8 and 6.5m. From 7-10 seconds, amplitudes decrease slightly to about 0.10g in the lower 2 accelerometers and input motion. At 7 seconds, the rate of pore pressure buildup increases in the 14.8m transducer, slows in the 11m transducer, and remains steady in the 6.9m transducer. At 10 seconds, strong shaking stops in the 1.5m accelerometer, and remains steady at all other depths. Pore pressures are 100 percent at 1.5m, 35 at 6.9m, 40 at 11m, and 70 percent at 14.8m.

At 26 seconds, pore pressures reach their maximum values of 100 percent for 6.9m and 95 percent for 11m. Input motions increase from 0.10g to 0.25g, and remain constant at 0.10g at 14.5m. Accelerations decrease to about 0.05g at 3.8, 6.5, and 11.3m. Accelerations reduce to near zero at 1.5m. Accelerations and pore pressures remain relatively constant at all depths through the end of shaking at 65 seconds. Little or no pore pressure dissipation is observed during the 21 seconds since shaking stopped.

More generally, in the model code 2 series, excess pore pressures rose fairly rapidly to 100 percent or near 100 percent of the initial vertical effective stress (R_u = 1) throughout the column within a few cycles. The acceleration time histories decrease in amplitude as the R_u approaches 1. Despite the higher density of the upper layer, excess pore pressures within it reach high levels.

As the effective vertical confining stress is increased, the pattern of behavior is initially repeated. Models 3a-3d in Table 2 were designed to have an initial vertical effective stress of 2 atm in the lower, looser layer. All series 3 models had 18.25m of dense sand, relative densities of 73-80 percent, on top of 8m of loose sand, relative densities of 34-54 percent. All series 3 models were fully submerged. Example results for this model series are shown in Figure 4, for model 3c. This model was normally consolidated. Accelerometer records

are shown for depths of 1, 5.5, 14.5, 18.3, 22.3, 25.8m, and the input motion depth of 27m. Pore pressure transducer records are shown for depths of 0.75, 5.3, 10.8, 14.4, 18, 22, and 25m. The input motions are applied at 0.54 Hz, and the fundamental period of the soil column is estimated to be 4x26.25m/300mps = 0.35 seconds.

The input motions ramped up to a maximum of 0.09g at 3 seconds and dropped down to a steady 0.06g for the rest of cycling. At 25.8m, accelerations peaked in the 2nd cycle at 0.14g, and remained constant at 0.12g for the remainder of cycling. At 22.3m, accelerations ramped up to 0.09g. Accelerations peaked at 0.035g in 4 seconds at 18.3m. At 5 seconds, accelerations peaked at 0.035g for 14.5m, 0.022g for 5.5m, and 0.036g for 1m. Pore pressures begin to rise at all depths as soon as shaking starts. There is no lag as observed at 1 atm. At 5 seconds, pore pressures are 100 percent at 0.75m, 80 percent at 5.3m, 70 percent at 10.8m, 55 percent at 14.4m, and 87 percent at 18, 22, and 25m. Pore pressures reached maxima of 100 percent in 5 seconds at 0.75m, 16 seconds at 5.3m, 22 seconds at 10.8m, 51 seconds at 14.4m, 7 seconds at 18 and 22m, and 30 seconds at 25m. After shaking stopped, excess pore pressures remained constant at 100 percent.

Above an initial vertical effective stress of around 250 –300 KPa (3 atm), however, a different behavior was observed. Under high effective confining stresses, it was noted that in many cases, excess pore pressures did not reach the initial vertical effective stress. Figure 5 shows the results from Model 4d, a deep soil column with a target vertical effective stress of 500 KPa (5 atm) near the bottom of the model. Model 4d was subjected to a relatively low level of shaking amplitude. Nevertheless, in the initial stages of shaking, the excess pore pressure development within the loose layer is positive. Within around 20 cycles, the excess pore pressure reached 45 percent of the effective overburden stress. Shortly after this, the rate of generation of pore pressures all but ceases. There is a slight reduction in the amplitude of the acceleration, reflecting the increase in excess pore pressure but the displacement (strain) cycles continue for a considerable period without further increase in excess pore pressure. One concern was that the low amplitude of shaking might be the reason for this plateau in pore pressure at only 45 percent of the initial vertical effective stress. Subsequent models similar to model 4d were tested with higher levels of input shaking, revealing the same pattern as shown in Figure 5.

Figure 6 shows the results of a model very similar to model 4d, shown in Figure 5, but now the model is homogeneous rather than a two layer case. Model 4j had slightly less weights used for surcharging resulting in an initial vertical effective stress near the bottom of the model of around 400 KPa (4 atm). Notice that the level of input shaking is more than double that of model 4d, from 0.11 g to 0.25 g. Pore pressure transducers located in the deep loose layer (33 m and 36 m depths) reach a limit of 78 percent for this case. The largest excess pore pressure (90 percent) occurs at a depth of 28.5 m.

A second homogeneous model was tested, without the use of weights for surcharging as was used in model 4j. The results of this test, model 4k, are shown in Figure 7. Model 4k depicts a 26 m deep homogeneous deposit of D_r = 49 percent clean sand. The input peak horizontal acceleration in the model was 0.31g. The model did not contain any lead weight surcharging; the increase in confining stress was accomplished by testing the model at increasing g levels. The results shown in Figure 7 are those from a 50g test, which produces an initial effective confining stress near the bottom of the model of 230 KPa (2.3 atm). As expected, with a confining stress of only 2.3 atm, the entire model liquefied. This model was also tested at higher g levels of 80g, 100g, and 125g, the results of the testing at 100g are discussed next.

Figure 8 shows the results of model 4k tested at a centrifugal acceleration of 100g, which produces an initial effective confining stress near the bottom of the model of 400 KPa (4 tsf). The results shown are after the model was initially tested (input shaking applied) at 50g, held at 50g for several minutes to allow the pore

pressures to dissipate, spun up to 80g and tested, held at 80g for several minutes to allow pore pressure dissipation, and then spun up to 100 g and tested. Pore pressures initially increase rapidly, and then more slowly, and reach 100 percent or near 100 percent of the vertical effective stress. At depths of 44.5 and 52 m, the pore pressures plateau at approximately 82 percent.

The last sets of data are presented in Figures 9 and 10, representing models 5a and 5d respectively. These results represent two-layer models surcharged with a large amount of lead weights and tested at 50g. For model 5a shown in Figure 9, the confining stress near the bottom of the deposit is 740 KPa (7.4 tsf). Peak input acceleration at the base is about 0.1g. In this test, the pore pressure transducers at depths of 50 and 53 m, corresponding to the relatively loose soil (relative density about 51 percent), reach a peak value of only about 50 percent, even with numerous additional cycles of loading. Very little to no excess pore pressure was recorded in the soil column above 50 m.

Nearly identical results are seen in Figure 10, model 5d. This model had slightly larger lead weights resulting in a confining stress near the bottom of the deposit of 920 KPa (9.2 tsf). The level of shaking was also increased from that applied in model 5a from 0.1 g to 0.3 g. At a depth of 63 m, the pore pressure peaked at a value of 55 percent, and at a depth of 59 m the pore pressure peaked at a value of 40 percent. Very little to no excess pore pressure was recorded in the soil column above 59 m.

4.0 DISCUSSION OF RESULTS

In the homogeneous models, excess pore pressures rise more quickly and to higher levels throughout the column than in the two-layer models. Post-shaking pore pressure redistribution is difficult to see because the whole column liquefied, so the gradients are smaller. These observations suggest that pore pressures are being generated cyclically within each layer (local generation) in addition to redistribution effects. The pore pressures do not reduce within 20 sec after shaking stops, so, dissipation is not observed. Also notice the sharp correspondence between accelerations and pore pressure responses. The sharp pore pressure peaks and liquefaction observations indicate that sufficient saturation was achieved with the employed model saturation and consolidation procedures.

The rate at which PWP is increasing in the shorter columns appears to be too fast to be explained by pore pressure redistribution (flow) alone. Rather, a pressure wave effect may be occurring in the column. Communication of a high increment of pore pressure originating in a lower layer may be nearly instantaneous throughout the soil column. Whereas consolidation requires drainage to take place, the initial response is essentially undrained, and the speed of propagation of a compressive wave in the pore fluid will be many times the velocity of the shear wave through the soil skeleton. Thus it is feasible for a pore pressure increment, which arises during part of a cycle of loading to be communicated upwards through the soil column in advance of the shear wave that created it. As the increments of excess pore pressure tend to be large at depth, then the potential impact on the response of the upper layer is increased.

The surcharge has a distinct effect on the behavior of the soil column. The effect appears to be even more pronounced in the two layer models. For the deep two-layer models, excess pore pressures are generated only in the deeper layers. Dissipation or redistribution effects can be seen in the pore pressure response during and after shaking stops.

5.0 SUMMARY AND CONCLUSIONS

The relationship between effective confining stress and liquefaction potential, in terms of cyclically induced excess pore water pressure, has been extensively studied in the laboratory using traditional triaxial, torsional and simple shear devices. The laboratory studies show that there is a less-than-linear increase in cyclic shear strength with increasing effective confining stress. Laboratory tests indicate that 100 percent pore pressure response (liquefaction) can occur at high confining stresses in the range 3 to 12

atm. At lower confining stresses, less than 3 atm, stress history strongly influences liquefaction resistance, K_σ relationships, and threshold cyclic shear strain required to develop high pore pressures.

Experiments were conducted by the ERDC Centrifuge Research Team to investigate effective confining stress effects on liquefaction potential of fine, clean, Nevada sand, under the boundary and loading conditions of a centrifuge model. For this test series, twenty-six level ground models with either a dense layer over a loose layer or homogeneous profile were tested in an equivalent-shear-beam box. Some models were subjected to sequential earthquakes, and some models were overconsolidated, to observe stress-history effects on pore pressure development. A representative number of the models tested have been reported in this paper.

6.0 REFERENCES

Arulmoli, K., Muraleetharan, K.K., Hossain, M.M., and Fruth, L.S., (1992). "VELACS Verification of Liquefaction Analyses by Centrifuge Studies Laboratory Testing Program Soil Data Report." National Science Foundation Report.

Butler, G.D., (1999). A dynamic analysis of the stored energy angular momentum actuator used with the equivalent shear beam container, PhD thesis, Cambridge University.

Steedman, R.S., (1999). Earthquake engineering support, Phase 3, Final Technical Report, N68171-99-C-9021, European Office of the U.S. Army, London, November.

Steedman, R.S., Ledbetter, R.H., and Hynes, M.E., (2000). "Liquefaction of sands under high initial effective confining stresses." Proc. GeoDenver 2000, ASCE Geotech. Spec. Pub., August.

Youd, L. and Idriss, I. M., Editors (1997). "Workshop on Evaluation of Liquefaction Resistance of Soils." Proceedings, Salt Lake City, Technical Report NCEER-97-0022, sponsored by FHWA, NSF and WES, published by NCEER

TABLE 1. Outline summary of centrifuge model test program

Model series	Models in series	Effective overburden stress near bottom	Equivalent field depth (approx)	Depth of specimen	Notes (all specimens constructed from Nevada Sand, tested at 50g unless indicated)
2	a, b, c, d, e, f	1 tsf	15 m	300 mm	Fully submerged
3	a, b, c, d, e	2 tsf	26 m	525 mm	Fully submerged
4	a, b, c, d	3 – 5 tsf	26 – 40 m	525 mm	Lowered water table or surcharge (weights)
	e, f, g, h, i, j	3.9 – 9.7 tsf	30 – 60 m	525 mm	Surcharge (weights) and change in g level, fully submerged
	k	1.9 – 4.8 tsf	25 – 39 m	525 mm	Change in g level, no surcharge, fully submerged
5	a, b, c, d, e	7 – 10 tsf	54 – 63 m	525 mm	Surcharge (weights), fully submerged

TABLE 2. Summary description of centrifuge model test program

Model Code	Dpth. (mm)	Relative Density (D_r)*	σ_v' near bottom of deposit (tsf)	OCR	Number of Eqks.	Comments: All models constructed from Nevada Sand and tested at 50g unless specified**
2a	300	44% loose, 83% dense	1	1	3	Fully submerged
2b	300	50% loose, 75% dense	1	1	2	Fully submerged
2c	300	49% loose, 74% dense	1	1	5	Fully submerged
2d	300	50% loose, 75% dense	1	1	4	Fully submerged
2e	300	49% loose, 73% dense	1	2.5	4	Fully submerged
2f	300	50% loose, 75% dense	1	2.5	4	Fully submerged
3a	525	34% loose, 73% dense	2	1	2	Fully submerged
3b	525	49% loose, 77% dense	2	1	3	Fully submerged
3c	525	49% loose, 79% dense	2	1	3	Fully submerged
3d	525	54% loose, 80% dense	2	2.5	4	Fully submerged
4a	525	49% loose, 80% dense	3	1	4	Saturated to top of loose layer only.
4b	525	56% loose, 74% dense	3	2.5	4	Saturated to top of loose layer only.
4c	525	50% loose, 75% dense	4.7	1	4	Fully submerged, surcharge (weights)
4d	525	50% loose, 68% dense	4.7	2.5	4	Fully submerged, surcharge (weights)
4e	525	47% uniform	3.9 – 7.8	1	2,1,1**	Fully submerged, surcharge (weights), **Shaking at 50, 80, 100g
4f	525	55% uniform	3.9 – 9.7	1	1,1, 2,1**	Fully submerged, surcharge (weights), **Shaking at 50, 80, 100, 125g
4g	525	50% uniform	3.9 – 9.7	1	1,1, 1,2**	Fully submerged, surcharge (weights), **Shaking at 50, 80, 100, 125g
4h	525	50% uniform	3.9 – 9.7	1	1,1, 1,1**	Fully submerged, surcharge (weights), **Shaking at 50, 80, 100, 125g
4i	525	50% uniform	3.9 – 9.7	1	1,1, 1,1**	Fully submerged, surcharge (weights), **Shaking at 50, 80, 100, 125g
4j	525	50% uniform	3.9 – 9.7	1	1,1, 1,2**	Fully submerged, surcharge (weights), **Shaking at 50, 80, 100, 125g.
4k	525	50% uniform	1.9 – 4.8	1	1,1, 1,2**	Fully submerged, no surcharge, **Shaking at 50, 80, 100, 125g.
5a	525	51% loose, 72% dense	7.4	1	4	Fully submerged, surcharge (weights)
5b	525	49% loose, 76% dense	7.4	2.5	4	Fully submerged, surcharge (weights)
5c	525	52% loose, 75% dense	9.2	1	3	Fully submerged, surcharge (weights)
5d	525	57% loose, 80% dense	9.2	1	1	Fully submerged, surcharge (weights)
5e	525	50% uniform	8.4	1	7	Fully submerged, surcharge (weights)

*Relative density of the portion of the model termed 'loose', always refers to a 160 mm thick layer at the bottom of the model. Relative density of the portion of the model termed 'dense', refers to that portion of the model above the 'loose' layer (ranges in thickness from 140 to 365 mm)

Table 3. Nevada Sand Properties (as measured)	
Specific Gravity	2.64
Maximum void ratio	0.757 (density 1502.53 kg/m^3)
Minimum void ratio	0.516 (density 1741.21 kg/m^3)
D_{50}	0.18 mm
D_{10}	0.11 mm

Table 4. Pore Fluid Properties (as measured)	
Density	1200 kg/cm^3
Viscosity	50 cs
Specific Gravity	1.26
Composition	85% glycerine, 15% water (by weight)

Table 5. Characteristics of Input Motion			
Model	**Freq., Hz**	**A_{max}, g**	**Number of cycles**
2f (Figure 3)	0.54	0.25	34
3c (Figure 4)	0.54	0.09	35
4d (Figure 5)	0.54	0.11	50
4j (Figure 6)	1.18	0.25	57
4k (50g), (Figure 7)	1.17	0.32	57
4k (100g), (Figure 8)	0.88	0.42	85
5a (Figure 9)	0.54	0.10	35
5d (Figure 10)	0.86	0.32	51

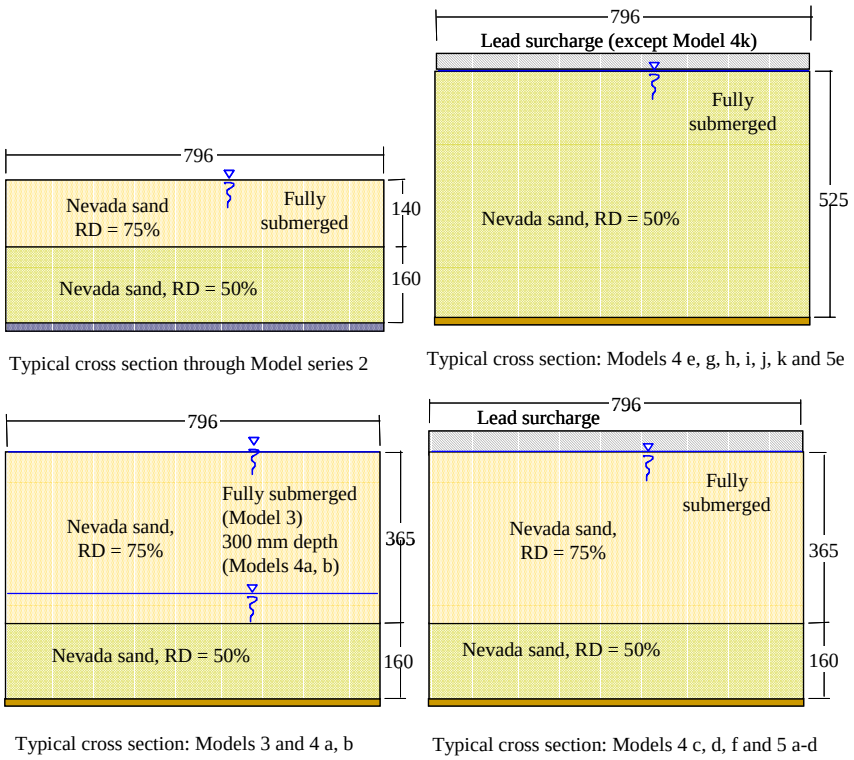

Figure 1. Cross sections through different centrifuge models (all dimensions in mm)

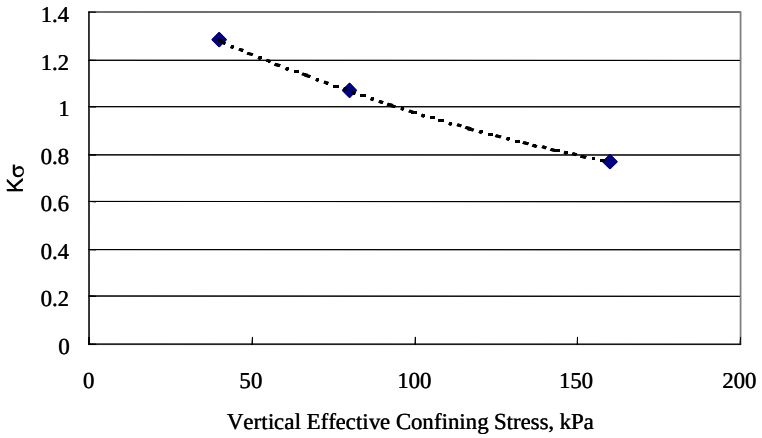

Figure 2. K_σ relationship for Nevada sand based on cyclic triaxial test data as reported by Arulmoli et al., 1992.

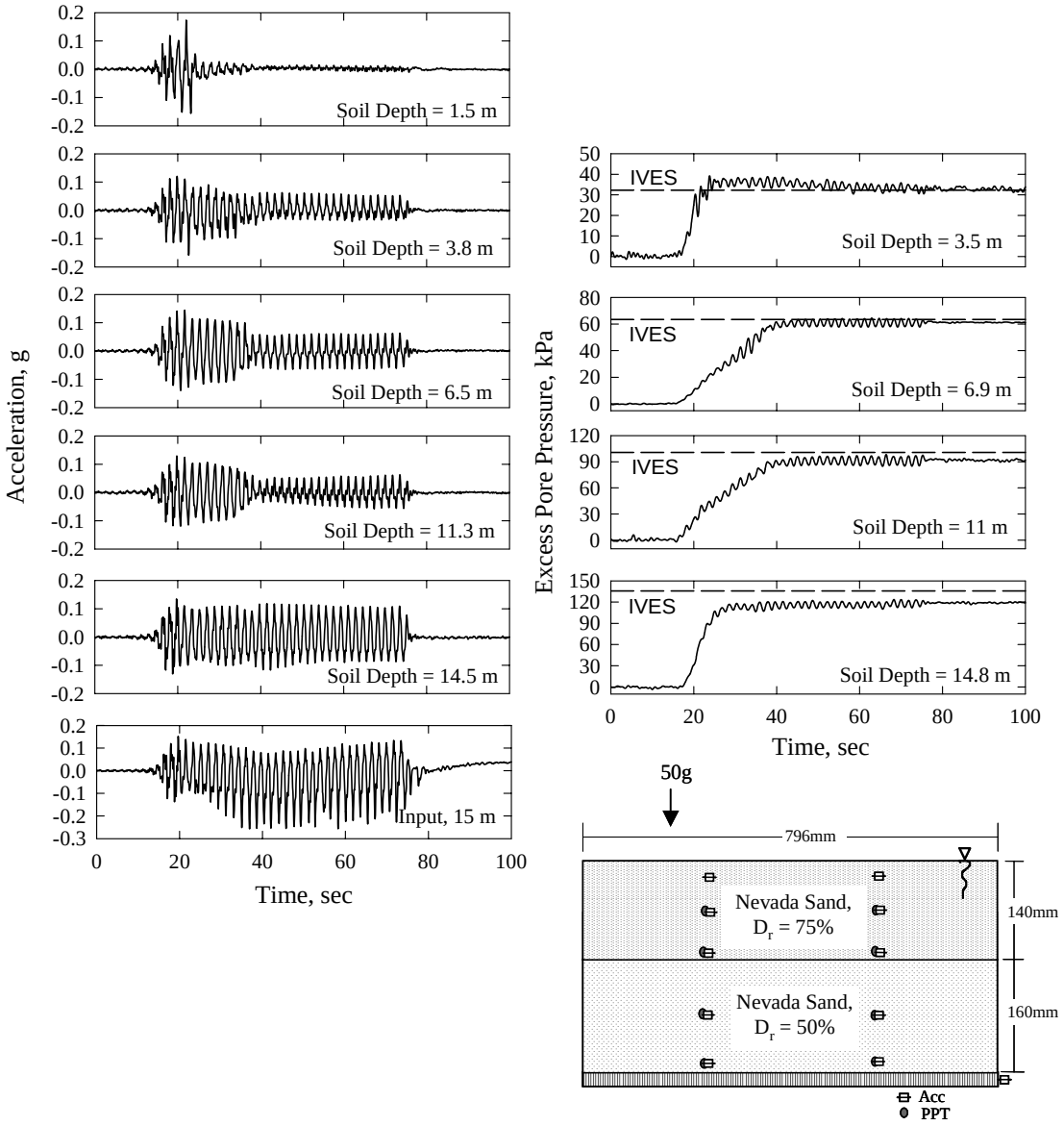

Figure 3. Results from model 2f showing recorded accelerations and excess pore pressure

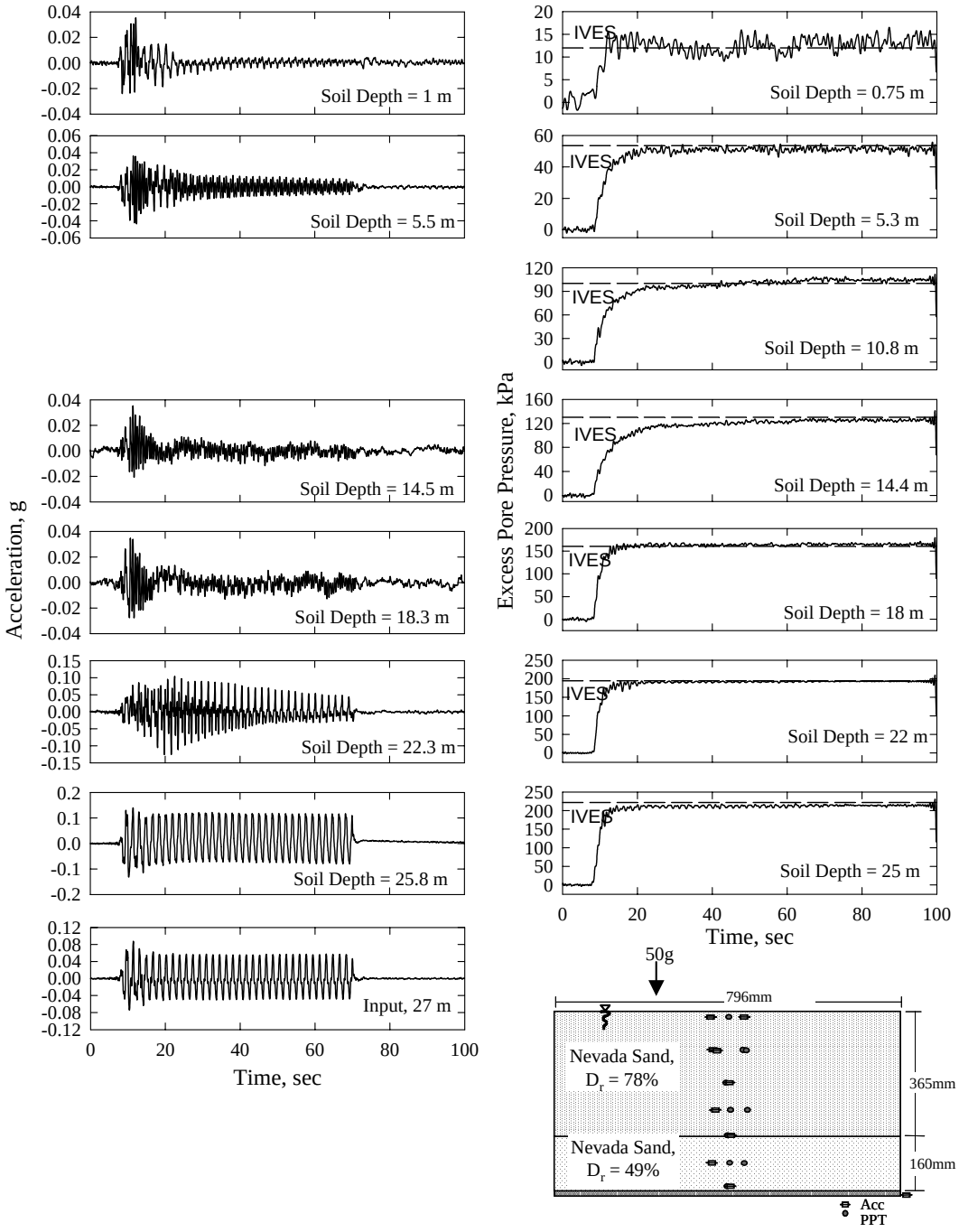

Figure 4. Results from model 3c showing recorded accelerations and excess pore pressure

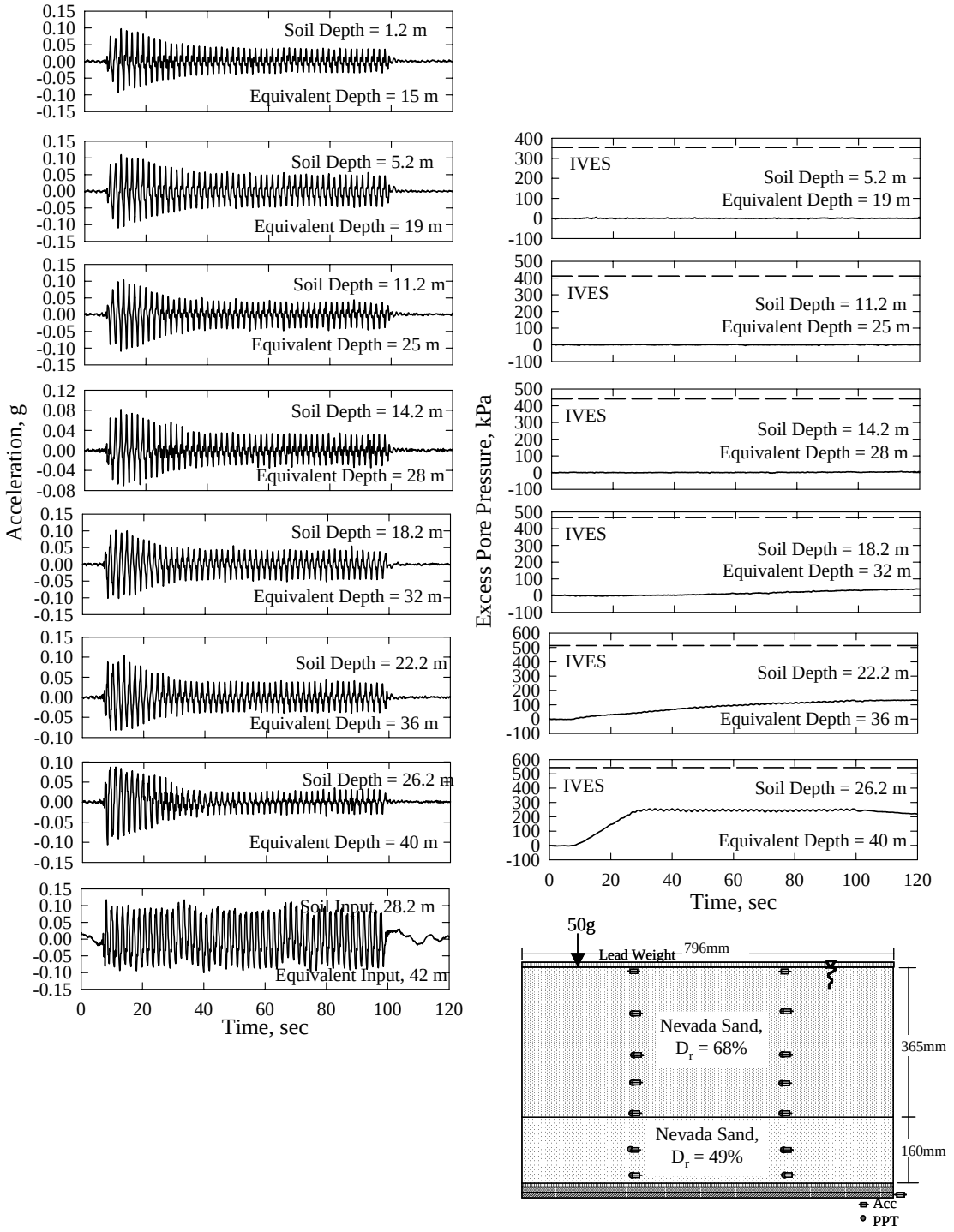

Figure 5. Results from model 4d showing recorded accelerations and excess pore pressure

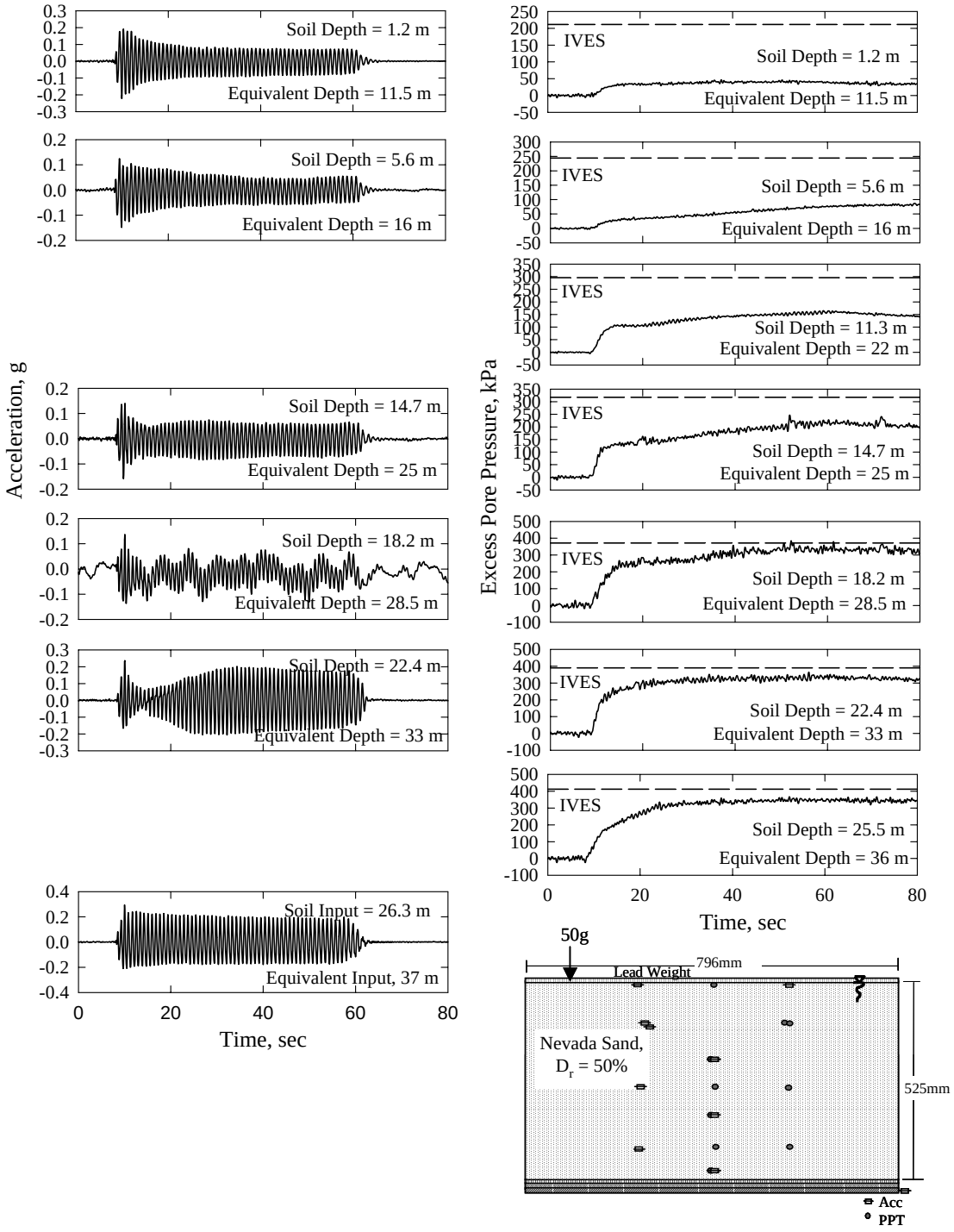

Figure 6. Results from model 4j showing accelerations and excess pore pressures.

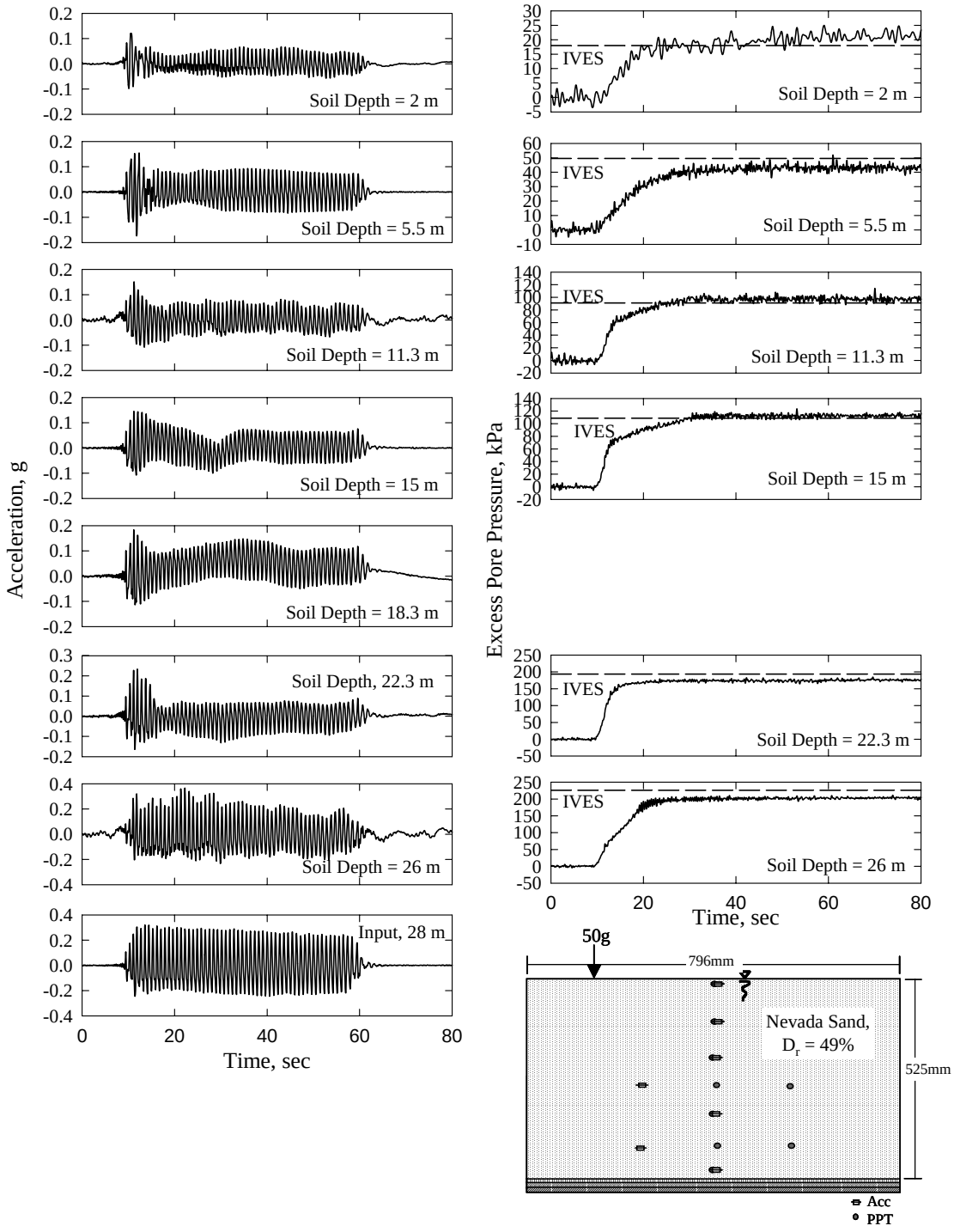

Figure 7. Results from model 4k, 50 g showing accelerations and excess pore pressure.

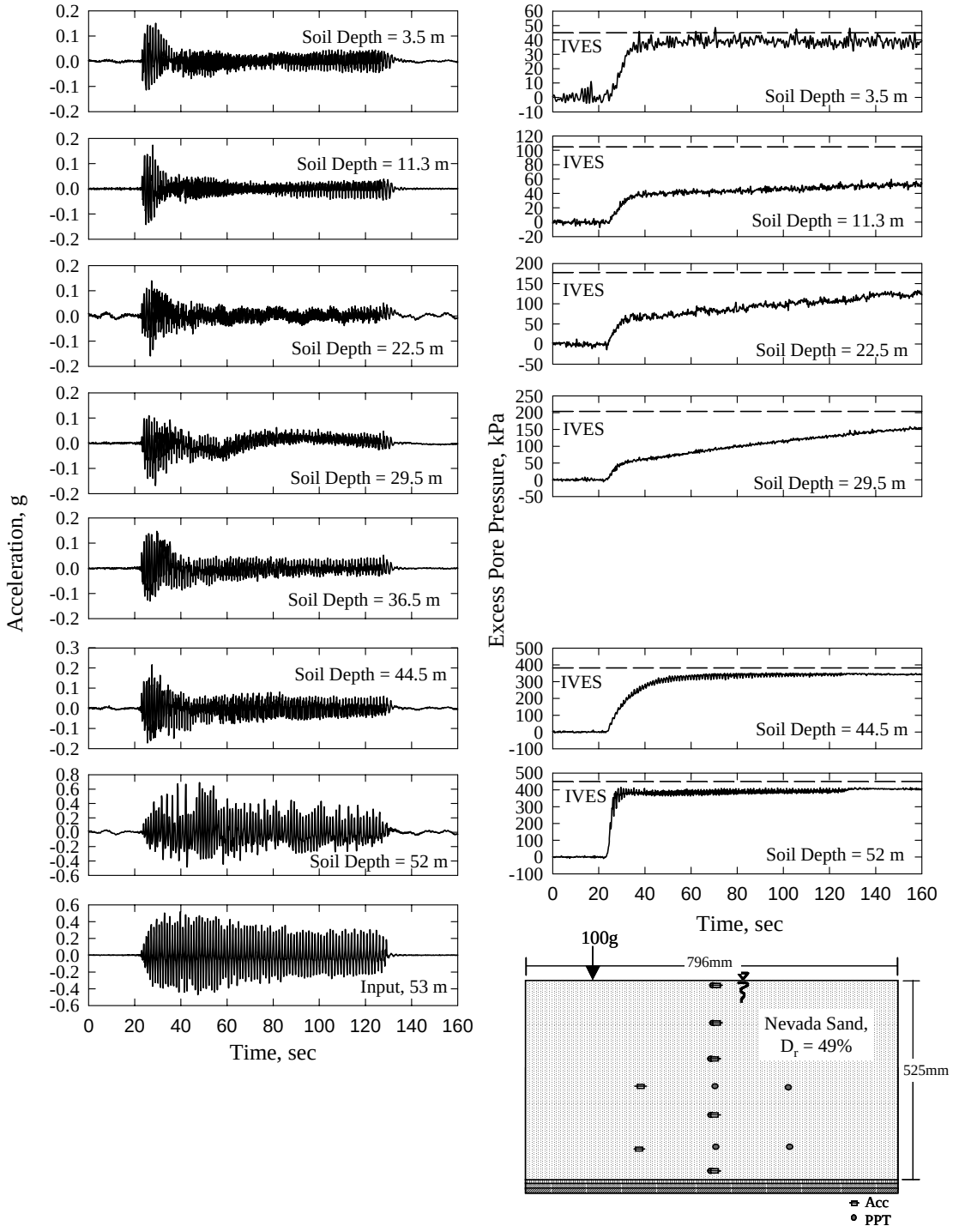

Figure 8. Results from model 4k, 100g showing accelerations and excess pore pressures.

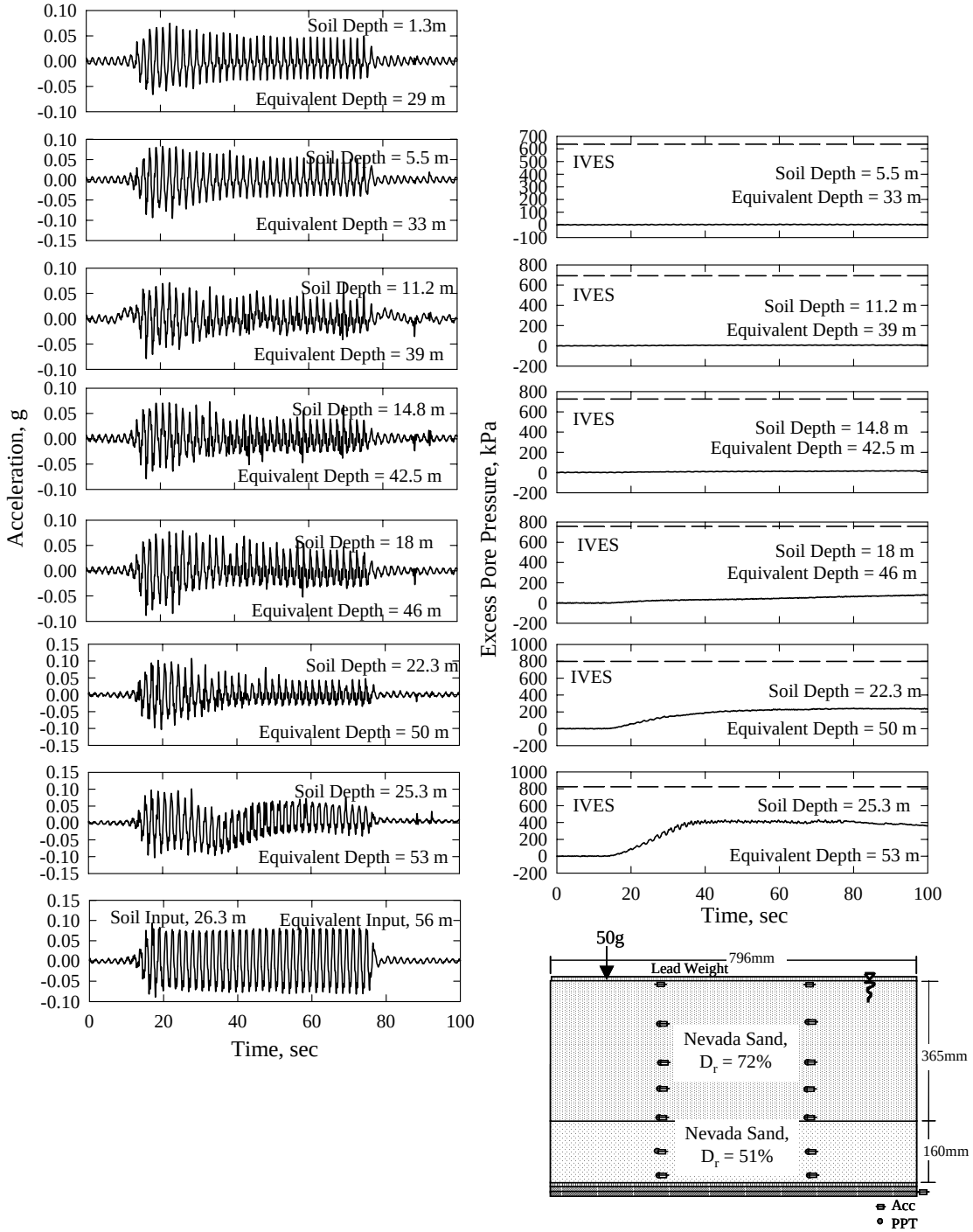

Figure 9. Results from model 5a showing accelerations and excess pore pressure.

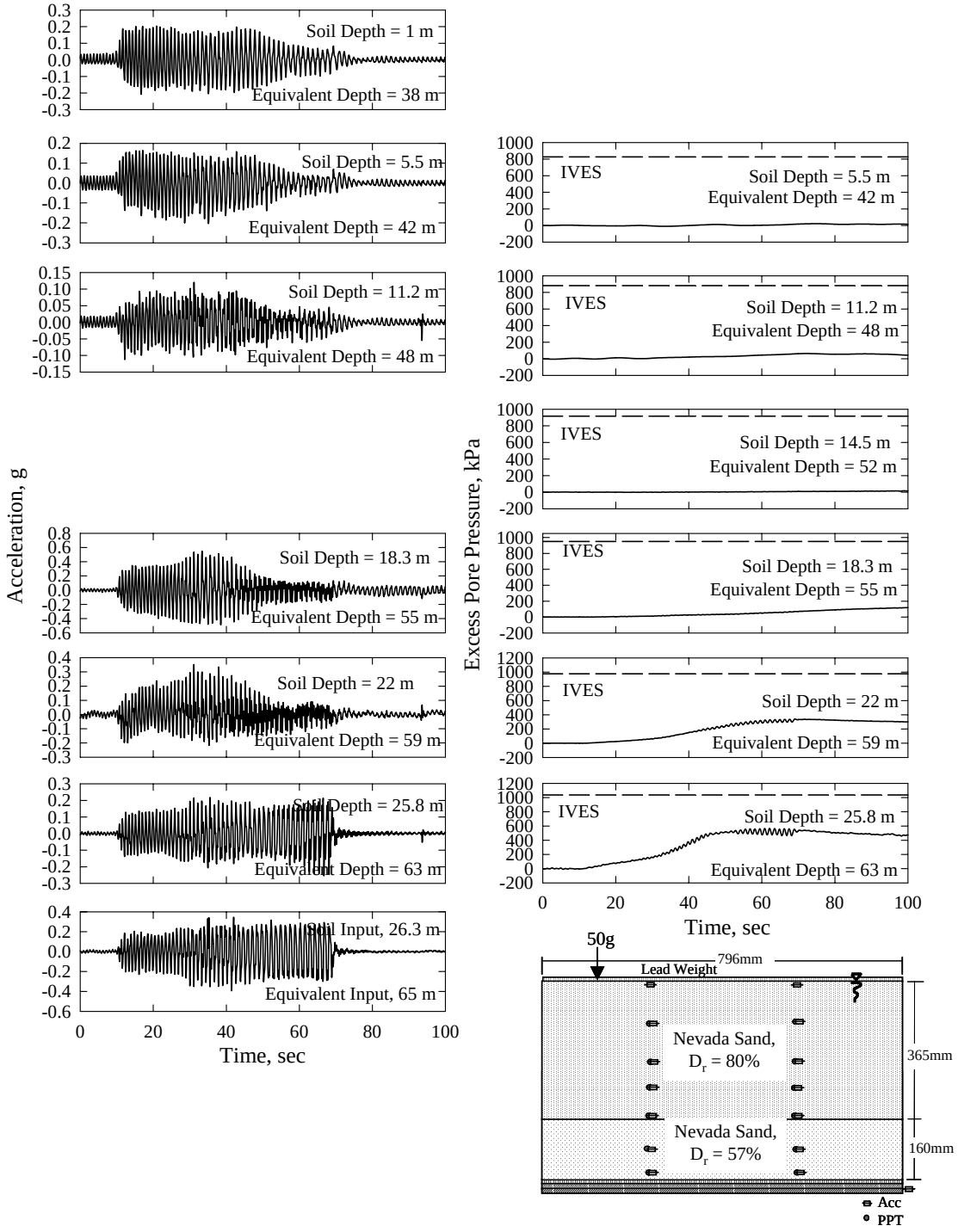

Figure 10. Results from model 5d showing accelerations and excess pore pressures.